Journal of Magnetism and Magnetic Materials 418 (2016) 122–127

Contents lists available at ScienceDirect

Journal of Magnetism and Magnetic Materials

journal homepage: www.elsevier.com/locate/jmmm

Investigation on structural, Mössbauer and ferroelectric properties of $(1-x)PbFe_{0.5}Nb_{0.5}O_3$–$(x)BiFeO_3$ solid solution

Sunanda T. Dadami [a], Shidaling Matteppanavar [a], Shivaraja I.[a], Sudhindra Rayaprol [b], Basavaraj Angadi [a,*], Balaram Sahoo [c]

[a] Department of Physics, JB Campus, Bangalore University, Bangalore 560056, India
[b] UGC-DAE-Consortium for Scientific Research, Mumbai Centre, BARC Campus, Mumbai 400085, India
[c] Materials Research Centre, Indian Institute of Science, Bangalore 560012, India

ARTICLE INFO

Article history:
Received 16 November 2015
Received in revised form
27 January 2016
Accepted 28 January 2016
Available online 29 January 2016

Keywords:
Single step method
X-ray diffraction
Antiferromagnetism
Mössbauer
Ferroelectric

ABSTRACT

In this study, $(1-x)PbFe_{0.5}Nb_{0.5}O_3$(PFN)–$(x)BiFeO_3$(BFO) multiferroic solid solutions with $x=0.0$, 0.1, 0.2, 0.3 and 0.4 were synthesized through single step solid state reaction method and characterized thoroughly through X-ray Diffraction (XRD), Scanning Electron Microscopy (SEM), Fourier Transform Infra-Red (FTIR), Raman, Mössbauer spectroscopy and ferroelectric studies. The room temperature (RT) XRD studies confirmed the formation of single phase with negligible amount of secondary phases ($x=0.2$ and 0.4). The zoomed XRD patterns of $(1-x)$PFN–(x)BFO solid solutions showed the clear structural phase transition from monoclinic (*Cm*) to rhombohedral (*R3c*) at $x=0.4$. The Raman spectra of the $(1-x)$PFN–(x)BFO solid solutions showed the composition dependent phase transition from monoclinic (*Cm*) to rhombohedral (*R3c*). With increasing x in PFN, the modes related monoclinic symmetry changes to those of rhombohedral symmetry. The RT Mössbauer spectroscopy results evidenced the existence of composition dependent phase transition from paramagnetic to weak antiferromagnetic ordering and weak antiferromagnetic to antiferromagnetic ordering. The Mössbauer spectroscopy showed paramagnetic behavior with a doublet for $x=0.0$, 0.1 and 0.2 are shows the weak antiferromagnetic with paramagnetic ordering. For $x=0.3$ and 0.4 shows the sextet pattern and it is a clear evidence of antiferromagnetism. The ferroelectric (P–E) loops at RT indicate the presence of small polarization, as the x concentration increases in PFN, the remnant polarization and coercive field were decreased, which may due to the increase in the conductivity and leaky behavior of the samples.

1. Introduction

Multiferroics are the materials in which at least two of the three ferroic properties, namely ferroelectricity, ferromagnetism and ferroelasticity, can coexist and are intrinsically coupled. Nowadays the term multiferroic has been generalized to include materials having antiferroic orders [1–3]. Due to the coupling between ferroelectric and magnetic domains, the multiferroic materials offer a new class of applications in multistage information storage devices like FeRAM, MRAM etc., [4]. However, in nature very few materials exhibit both spontaneous magnetization and electric polarization simultaneously. This is due to the fact that the magnetic ordering requires partially filed electrons in the 'd' orbital whereas empty 'd' orbital for the ferroelectricity. Among them $PbFe_{0.5}Nb_{0.5}O_3$ (PFN) is a well-known $A(B'_{1/2}B''_{1/2})O_3$ type multiferroic, has received considerable attention in technical applications due to its potential. PFN was considered to be ferroelectrically and antiferromagnetically ordered below its Néel temperature ($T_N \sim 155$ K) [5]. The PFN undergoes a phase transition from paraelectric (PE) to ferroelectric (FE) at Curie temperature (T_C) around 385 K [6,7].

The multiferroic properties of PFN have been reported by various researchers from the beginning. Recently, Bonny et. al. [8], Lampis et. al. [9], Singh et. al. [2], and Matteppanavar et. al. [5] discussed the multiferroics properties of PFN at below 155 K and structure reported was monoclinic with *Cm* space group. In order to improve magnetic properties and to enhance the Néel temperature of PFN, many efforts are made [10,11,12,13]. Here we are made an attempt to synthesize the solid solution of PFN with other perovskite structure having T_C and T_N above room temperature.

The $BiFeO_3$ (BFO) is only room temperature multiferroic on which basis such solid solutions are formed. It has got the highest ferroelectric polarization (50–100 μC/cm^2 measured on insulating

* Corresponding author.
E-mail address: brangadi@gmail.com (B. Angadi).

http://dx.doi.org/10.1016/j.jmmm.2016.01.092
0304-8853/

single crystals) [14,15], ferroelectric Curie temperature (T_C ~1103 K) [16] and Néel temperature (T_N~643 K) [17] for G type antiferromagnetism with an incommensurate cycloidal magnetic ordering in the [110] direction [17,18]. In addition, the bulk BFO is characterized by serious leakage current problems due to the existence of large number of charge centers caused by oxygen ion vacancies and Bi_2O_3 evaporation during sintering process which makes it difficult to achieve high resistivity. These problems limit the use of BFO for fabrication of multifunctional devices.

Due to these problems, various attempts have been made by researchers to obtain BFO based multiferroic materials with improved magnetic, electric and magnetoelectric (ME) properties. The solid solutions of BFO with other perovskite type ferroelectric materials like $BaTiO_3$, $PbTiO_3$, $PrFeO_3$ and $PbFe_{0.5}Nb_{0.5}O_3$ exhibited enhanced spontaneous magnetization [19–22]. Recently, Patel et. al. [23] reported the solid solution of $Pb(Fe_{0.5}Nb_{0.5})O_3$–$BiFeO_3$ and observed the enhanced magnetic and electric properties. We endeavored to look for the solid solutions of $(1-x)$PFN–(x)BFO to stabilize the single phase and to improve the magnetic and ferroelectric properties. In this work, we employed a single step solid state reaction method to achieve single phase $(1-x)$PFN–(x)BFO solid solution with $x=0.0$ to 0.4. Synthesized solid solutions are characterized through various techniques to study the structural, Mössbauer and ferroelectric properties

2. Experimental

2.1. Sample preparation and characterization

The single phase $(1-x)$PFN–(x)BFO solid solutions ($x=0.0$, 0.1, 0.2, 0.3 and 0.4) were synthesized through the single step solid state reaction technique. Analytic reagent (AR) grade chemicals, $Pb(NO_3)_2$, Bi_2O_3, Fe_2O_3 and Nb_2O_5, with minimum assay of 99%, were used for the synthesis of single phase $(1-x)$PFN–(x)BFO solid solutions.

The PbO and Bi_2O_3 are the highly volatile at 850 °C and above and in order to maintain the stoichiometry in the samples during synthesis excess $Pb(NO_3)_2$ and Bi_2O_3(1%) were added. The detailed synthesis method is explained elsewhere [5,24]. The starting materials were dry mixed and then ground using agate pestle and mortar in an ethanol medium for 2 h. The obtained fine powder was calcined in a closed alumina crucible at 700 °C for 2 h and pressed into pellets of 10 mm diameter and 2 to 3 mm thickness under a pressure of 50 kN with 5% Polyvinyl Alcohol (PVA) as a binding material. To optimize the single phase we used the Pb and Bi rich environment. The pellets were used for the sintering for different temperatures 800 °C, 850 °C, 900 °C, 950 °C, 1000 °C and 1050 °C for 1 h. Among all these conditions we observed less secondary phase at 800 °C. After this we increased the sintering duration from 1 to 5 h by keeping 800 °C constant. In these conditions, single phase was achieved for $(1-x)$PFN–(x)BFO solid solutions at 800 °C.

The phase purity of the materials was examined through XRD using Phillips (1070 model) diffractometer with Cu Kα (1.5406 Å) radiation. The data were recorded at RT between 2θ range 20° and 80° with step size of 0.02°. The volume fraction of the pyrochlore (%) is calculated from the XRD of each sample using the relative integrated intensities of the (222) pyrochlore peak I_{pyro} and the (110) perovskite peak I_{perov}.

$$\text{Volume fraction of pyrochlore (\%)} = \frac{(I\text{pyro})}{(I\text{pyro} + I\text{perov})} x\ 100$$

The SEM was used for the study surface morphology of the samples. Fourier Transform Infrared (FTIR) spectra of all the solid solutions were recorded at RT using Bruker Tensor 27 spectrometer. Raman spectra were collected at RT using Ocean Optics Micro Raman spectrometer (Dunedin, USA) with a back-scattering configuration and the excitation laser wavelength of 785 nm and with an output power of 70 mW. Transmission Mössbauer spectra was measured at RT by using a ^{57}Co radioactive source mounted on a constant acceleration Mössbauer drive from SEE Co., USA and a proportional counter. The Mössbauer spectrum was analyzed with the computer program NORMOS written by Brand [25]. Ferroelectric (P–E) loop measurements were carried out at RT by a ferroelectric loop tracer Precision Premier II, Radiant Technologies, USA.

3. Results and discussion

3.1. Structural studies: X-ray diffraction

Fig. 1 shows the RT XRD patterns of $(1-x)$PFN–(x)BFO solid solutions with $x=0.0$, 0.1, 0.2, 0.3 and 0.4. It was found that all the solid solutions exhibit single phase. However, for $x=0.2$ and 0.4 a small amount of pyrochlore was found and it was estimated to be around 2.2% and 2.4%, respectively. The pyrochlore phase was identified as $Pb_2Nb_2O_7$. The low temperature sintering along with closed Pb and Bi rich environment helps in minimizing the evaporation of PbO and Bi_2O_3.The various calcination and sintering temperature and time duration were tried to achieve single phase and the optimized annealing parameters are 700 °C/2 h calcination and sintering at 800 °C/3 h.

The XRD pattern of pure PFN ($x=0.0$) is matching well with the monoclinic symmetry with *Cm* space group [26] and with increase of x from 0.0 to 0.4, the structure is observed to change from monoclinic (*Cm*) to disordered rhombohedral (*R3c*) structure. The

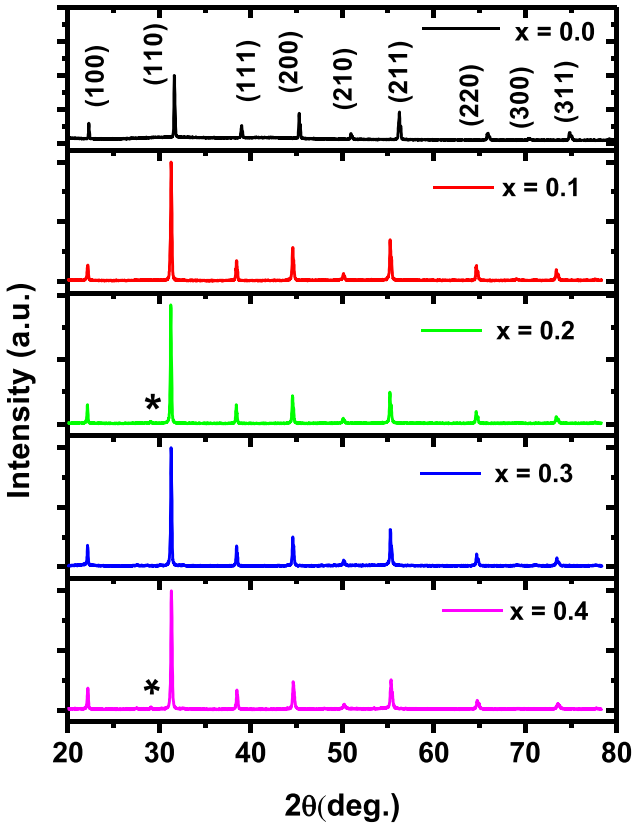

Fig. 1. XRD patterns of $(1-x)$PFN–(x)BFO solid solutions with $x=0.0$, 0.1, 0.2, 0.3 and 0.4 for 2θ range 20–80°. * corresponds to pyrochlore $Pb_2Nb_2O_7$ phase for $x=0.2$ and 0.4.

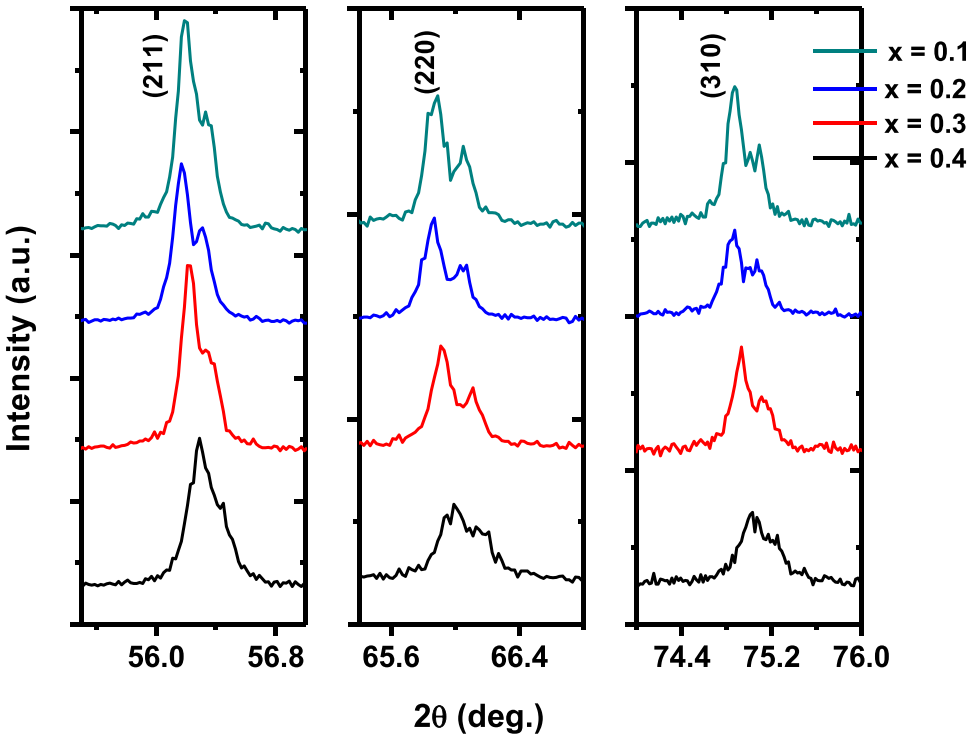

Fig. 2. Magnified views of XRD patterns of $(1-x)$PFN–(x)BFO solid solutions with $x=0.0$, 0.1, 0.2, 0.3, and 0.4.

structure of BFO is known to be rhombohedral with *R3c* space group [27]. Fig. 2 shows the zoomed view of (211), (200) and (310) reflections for $x=0.0$, 0.1, 0.2, 0.3 and 0.4.These reflections clearly show the doublet feature with the appearance of a shoulder and it is the direct evidence for the existence of monoclinic structure with *Cm* space group. With the increase of *x*, the intensity of the shoulder decreases and merges into a single broad peak at $x=0.4$. This clearly indicates the existence of structural phase transition from monoclinic to disordered rhombohedral. Also, the intensity of the (211), (200) and (310) reflections decrease with increase in *x*. The merging of peaks, shift in peak position, decrease in peak intensity and peak broadening are noticed with increase in *x*. The effect of rhombohedral structure was not observed much in the diffraction patterns may be due to the lower concentration of *x*. This study confirms the initiation of phase transition at $x=0.4$.

3.2. Structural studies: Raman spectroscopy

Fig. 3 shows the RT Raman spectra of $(1-x)$PFN–(x)BFO for $x=0.0$, 0.1, 0.2, 0.3 and 0.4 solid solutions. The general aspects of the Raman spectra show a marked change with the increase of *x*, which indicates a continuous change in symmetry. The bands between 500 and 900 cm^{-1} are known to be the key features for evaluating the B site order in Pb based multiferroics [28,29]. The modes located in the region 700–850 cm^{-1} corresponds to stretching vibrations of oxygen octahedra around Fe/Nb atoms of A1g (780.7 cm^{-1}), Eg (830.2 cm^{-1}) and F1u (704.4 cm^{-1}) symmetry of monoclinic phase. The region 400–530 cm^{-1} involves the bending O–Fe/Nb–O vibrations of F2g (536.8 cm^{-1}) and F1u (455.7 and 424 cm^{-1}) symmetry. The modes at the region 200–400 cm^{-1} are related to Pb–O bond stretching vibrations of F2u symmetry (290.3 cm^{-1}), Fe/Nb cation localized mode of F1u symmetry (255.4 and 298.1 cm^{-1}) and the rotational mode of Fe/Nb–O_6 octahedra of F1g symmetry (209.6 cm^{-1}). With the increase in *x*, all these monoclinic modes are slightly disappeared and $x=0.4$ confirms the slightly disordered rhombohedral phase with *R3c* space group. Recently, Singh et. al reported the

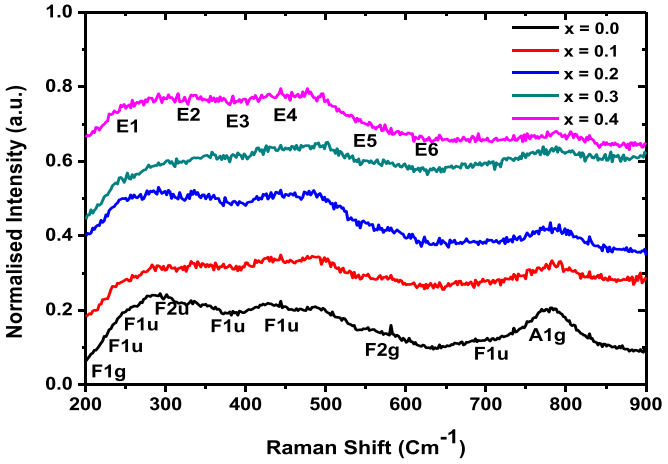

Fig. 3. Raman spectra of $(1-x)$PFN–(x)BFO solid solutions with $x=0.0$, 0.1, 0.2, 0.3 and 0.4.

rhombohedral Raman modes for BFO [30] with the observed six E modes at 275, 335, 365, 456, 549 and 597 cm^{-1} having weak average intensity of scattering. In the above six E modes 456 cm^{-1} is more reflecting in Fig. 3. This confirms the existence of rhombohedral (*R3c*) structure at $x=0.4$ and this corroborates well with the XRD (Fig. 2) results.

3.3. FTIR and SEM studies

FT-IR spectra of all samples are shown in Fig. 4 in the wave number range of 400–800 cm^{-1}.The broad absorption bands near 420 cm^{-1} and 526 cm^{-1} for all samples are due to overlapping of bismuth oxide and iron oxide in bending and stretching modes of vibrations which confirms the formation of perovskite structure. The absorption peaks at 526 cm^{-1} and 420 cm^{-1} are characteristics of O–Fe–O stretching and bending vibrations of FeO_6 respectively, in perovskite structure [31,32]. The absorptions at

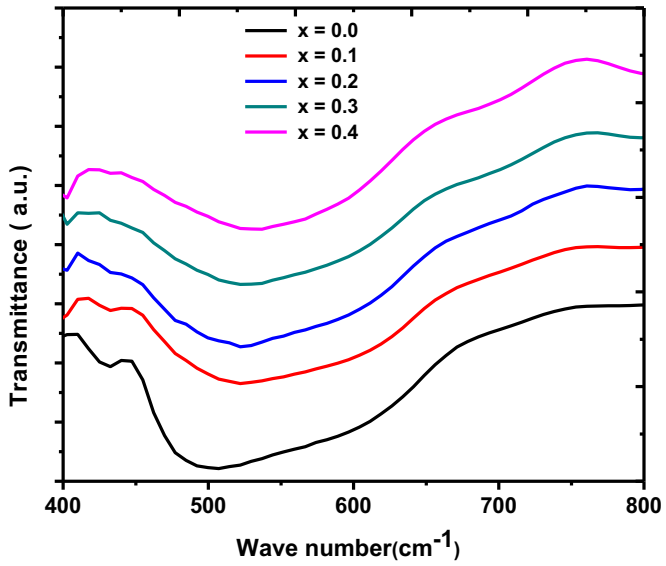

Fig. 4. FT-IR spectra of $(1-x)$PFN–(x)BFO solid solutions with $x=0.0$, 0.1, 0.2, 0.3 and 0.4.

420 cm^{-1} may be attributed to the stretching and bending vibrations of BiO_6 octahedra. Also, with increase in x content, there is a significant shift of absorption peak from 502 cm^{-1} to 526 cm^{-1} and is an indirect evidence of structural phase transition from monoclinic to disordered rhombohedral. Fig. 5 shows the SEM micrographs for the study of morphology of the solid solutions for $x=0.0$, 0.1, 0.2, 0.3 and 0.4. They show well-developed grains of irregular sizes and are homogeneously distributed throughout the sample with certain degree of porosity. The average grain size is found to be varying from 0.5 to 5 μm.

3.4. Mössbauer spectroscopy studies

^{57}Fe Mössbauer spectroscopy is one of the most efficient tools to investigate the local magnetic ordering, behavior and oxidation state of the iron (Fe) atoms in the structure. Fig. 6 shows the RT Mössbauer spectroscopy of $(1-x)$PFN–(x)BFO with $x=0.0$, 0.1, 0.2, 0.3 and 0.4 solid solutions and table 1 shows various parameters extracted from the measurement. From Fig. 6 it is clear that the spectrum is a Zeeman split six line pattern, where the black dots represent the experimentally recorded data points and the solid line is the least square fit to the measured data. The poor statistics is due to the absorption coefficients of lead for the Mössbauer is 14.4 keV for gamma rays.

The spectrum was fitted with a distribution of magnetic hyperfine fields P (Bhf). In the fitting, the line shape was assumed as Lorentzian. The hyperfine field distribution is shown on the right hand side of Fig. 6. It is expected that PFN shows the paramagnetic behavior through the doublets with isomer shift (Is)$=0.29\pm0.02$ mm/s and quadrupole shift (Qs)$=0.37\pm0.02$ mm/s correspond to Fe^{+3} in an octahedral environment. With the increase in x, the magnetic ordering shows a systematic change. At RT the sample $x=0.1$ shows paramagnetic ordering. From $x=0.2$ and onwards, we can see the origin of magnetic ordering in the sample, which clearly indicates phase transition from the paramagnetic to antiferromagnetic ordering. The $x=0.3$ and 0.4 samples show the above RT antiferromagnetic ordering. During the fitting, it is assumed that Fe^{+2} and Fe^{+3} ions are present and the resulting spectrum was fitted by Lorentzian. The nonzero electric quadrupole splitting demonstrates that Fe and Nb ions occupy non cubic off center sites and are randomly disordered around the B sites of the perovskite octahedra.

3.5. Ferroelectric studies

Fig. 7 illustrates the P–E hysteresis loops of $(1-x)$PFN–(x)BFO with $x=0.0$, 0.1, 0.2, 0.3 and 0.4 solid solutions. The ferroelectric loops were measured at room temperature with maximum applied electric field (E_m) of $\pm$15 kV/cm. The ferroelectric character of all solid solutions at room temperature has been evidenced by the observation of nearly saturated polarization loops. All the compositions show distinct hysteresis characteristics. Because of the different breakdown fields for different samples, varied drive fields were applied. For the samples with $x=0.0$, 0.1, 0.2, 0.3 and 0.4 the remnant polarization are Pr$=2.259$ μC/cm^2, 0.403 μC/cm^2, 0.196 μC/cm^2, 0.0983 μC/cm^2 and 0.0651 μC/cm^2 and coercive

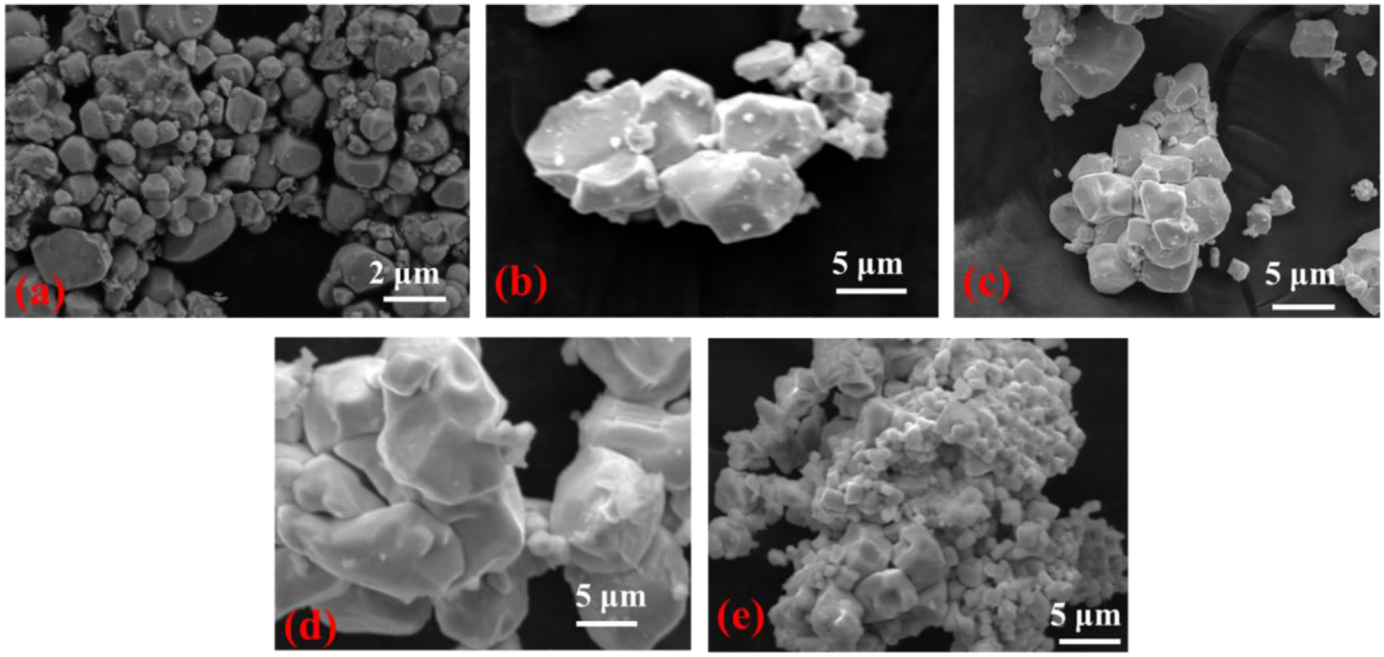

Fig. 5. Scanning electron micrographs of $(1-x)$PFN–(x)BFO solid solutions, (a) $x=0.0$, (b) $x=0.1$, (c) $x=0.2$, (d) $x=0.3$ and (e) $x=0.4$.

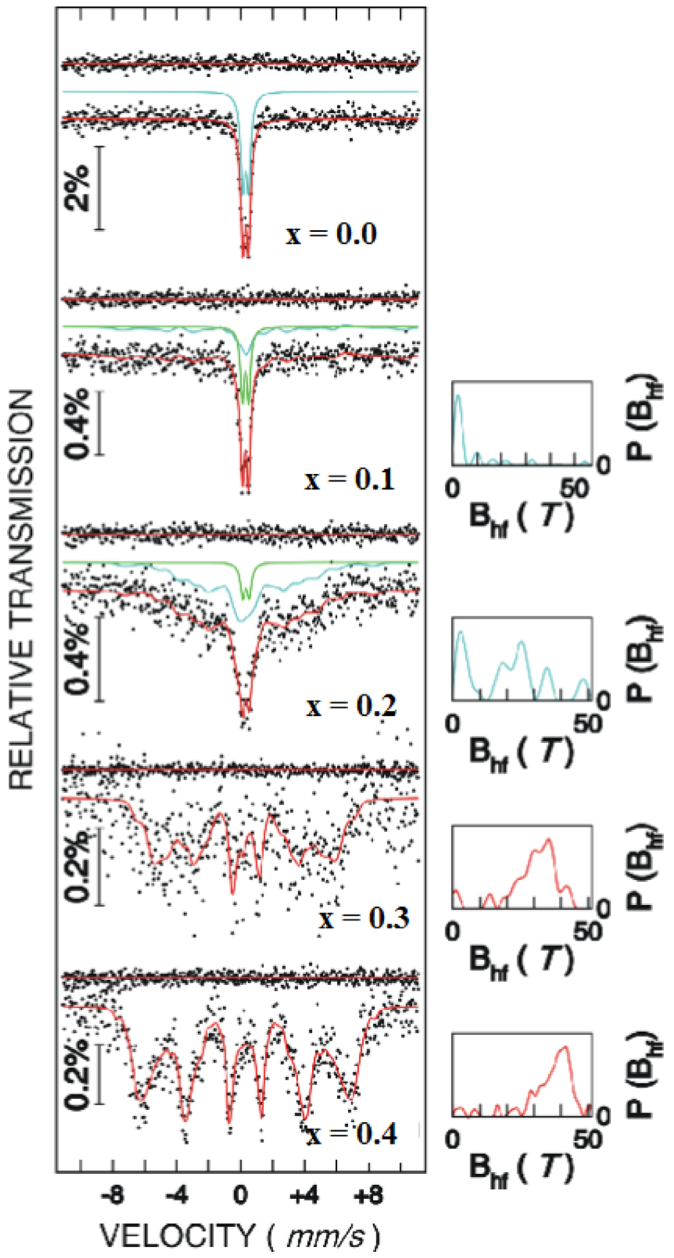

Fig. 6. Room temperature Mössbauer measurements of $(1-x)$PFN–(x)BFO solid solutions with $x=0.0$, 0.1, 0.2, 0.3 and 0.4.

Table 1
Various parameters extracted from the Mössbauer measurement.

Composition	Isomer shift (IS mm/s)	Quadrupole shift (QS mm/s)
$x=0.0$	0.304	0.375
$x=0.1$	0.200	0.024
$x=0.2$	0.229	0.055
$x=0.3$	0.132	0.661
$x=0.4$	0.240	0.018

fields are $E_c=7.731$, 4.016, 2.5629, 2.485 and 1.3345 kV/cm, respectively. The above results indicate that as the x concentration increases the remnant polarization and coercive field value decreases, which may be due to the increase in the conductivity and leakage current. The leakage current generated could be due to the presence of oxygen vacancies and mixed valence states of B-site cations in ABO_3 perovskite ferroelectric materials.

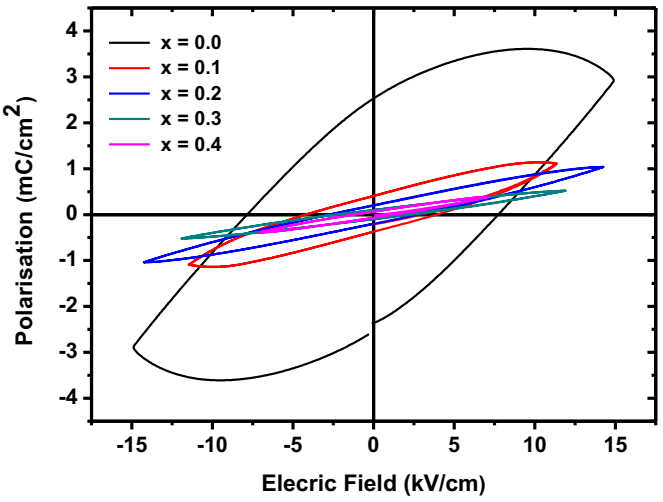

Fig. 7. Ferroelectric hysteresis (P–E) loops of $(1-x)$PFN–(x)BFO solid solutions at $x=0.0$, 0.1, 0.2, 0.3, and 0.4.

4. Conclusions

In summary, we successfully synthesized the single phase $(1-x)$PFN–(x)BFO solid solutions with $x=0.0$, 0.1, 0.2, 0.3 and 0.4 by single step solid state reaction method and investigated the structural, Mössbauer and ferroelectric properties at RT. It is observed that, with increase of x there is structural phase transition from monoclinic ($x=0.0$) to distorted rhombohedral ($x=0.4$). The grain size is found to be varying from 0.5 to 5 μm. Raman studies showed a clear evidence of phase transition from monoclinic to rhombohedral. The RT Mössbauer spectra shows paramagnetic ordering for $x=0.0$ and $x=0.1$. The magnetic ordering originates above $x=0.2$, indicating a phase transition from the paramagnetic to antiferromagnetic ordering. The $x=0.3$ and 0.4 samples show the above RT antiferromagnetic ordering. With the increase in x, the width of the line and isomer shift was found to change systematically and is due to the increasing Fe ratio in the sample that can lead to the enhancing of magnetic ordering towards room temperature and also cation ordering in the sample. Ferroelectric measurements showed the decrease in remnant polarization and coercive field as x increases, which may be due to the conducting and leaky behavior of the sample. These solid solutions could be potentially used for RT and above RT multifunctional devices.

Acknowledgments

The author SD would like to thank UGC (FIP) for its financial support. Also authors (SM, SI and BA) thank UGC-DAE-CSR, Mumbai Centre for providing financial support and experimental facilities through CRS-M 159 and CRS-M 200. SD, SM and BA, would like to thank DSTPURSE program for providing the Raman Spectroscopy measurement facility at Department of Physics, Bangalore University, Bengaluru. Authors also thank R. N. Bhowmik, Department of Physics, Pondicherry University Pondicherry for Ferroelectric measurements and Dr. M. V. Murugendrappa, B. M. S. College of Engineering Bengaluru for SEM measurements.

References

[1] W. Eerenstein, N.D. Mathur, J.F. Scott, Multiferroic and magneto electric materials, Nat. Mater. 442 (2006) 759–765.
[2] S.P. Singh, D. Pandey, S. Yoon, S. Baik, N. Shin, Resolving the characteristics of morphotropic phase boundary in the $(1-x)Pb(Fe_{1/2}Nb_{1/2})O_3$–$(x)PbTiO_3$

system: a combined dielectric and synchrotron x-ray diffraction study, Appl. Phys. Lett. 93 (2008) 182910(1)–182910(3).
[3] H. Schmid, Multi-ferroic magnetoelectrics, Ferroelectrics 162 (1994) 317–338.
[4] S.W. Cheong, M. Mostovoy, Multiferroics magnetic twist for ferroelectricity, Nat. Mater. 6 (2007) 13–20.
[5] S. Matteppanavar, B. Angadi, S. Rayaprol, Low temperature magnetic studies on $PbFe_{0.5}Nb_{0.5}O_3$ multiferroic, Physica B 448 (2014) 229–232.
[6] G.A. Smolenskii, I.E. Chupis, Ferroelectromagnets, Sov. Phys. Uspekhi 25 (1982) 475–493.
[7] G.L. Platonov, L.A. Drobyshev, Y.Y. Tomashpolskii, Y.N. Venevtsev, Electron diffraction and X-ray-diffraction investigation of atomic displacements in ferromagnet $Pb(Fe_{0.5}Nb_{0.5})O_3$, Sov. Phys. Crystallogr. 14 (1970) 692–695.
[8] V. Bonny, M. Bonin, P. Sciau, K.J. Schenk, G. Chapuis, Phase transitions in disordered lead iron niobate: X-ray and synchrotron radiation diffraction experiments, Solid State Commun. 102 (1997) 347–352.
[9] N. Lampis, P. Sciau, A.G. Lehmann, Rietveld refinements of the paraelectric and ferroelectric structures of $PbFe_{0.5}Nb_{0.5}O_3$, J. Phys. Condens. Matter 11 (1999) 3489–3500.
[10] B.H. Lee, N.K. Kim, J.J. Kim, S.H. Cho, Dielectric characteristics of $Pb[Fe_{1/2}(Ta,Nb)_{1/2}]O_3$ perovskite ceramic system, J. Korean Phys. Soc. 32 (1998) 978–980.
[11] C.J. Choi, W.K. Choo, C.K.K. Choo, Null thermal expansion behaviour of pseudo binary $(1-x)Pb(Fe_{1/2}Ta_{1/2})O_3$–$xPb(Mg_{1/2}W_{1/2})O_3$ and $(1-x)Pb(Fe_{1/2}Nb_{1/2})O_3$–$xPb(Mg_{1/2}W_{1/2})O_3$ solid solutions, Solid State Commun. 59 (1986) 245–247.
[12] M. Yokosuka, Electrical, Electromechanical and Structural Studies on Solid Solution Ceramic $Pb(Fe_{1/2}Nb_{1/2})O_3$–$Pb(Zn_{1/3}Nb_{2/3})O_3$, Jpn. J. Appl. Phys. 38 (1999) 5488–5492.
[13] I. Grinberga, M.R. Suchomel, P.K. Davies, A.M. Rappe, Predicting morphotropic phase boundary locations and transition temperatures in Pb- and Bi-based perovskite solid solutions from crystal chemical data and first-principles calculations, J. Appl. Phys. 98 (2005) 094111(1)–094111(10).
[14] V.V. Bhat, B. Angadi, A.M. Umarji, Synthesis, low temperature sintering and property enhancement of PMN-PT ceramics based on the dilatometric studies, Mater. Sci. Eng. B 116 (2005) 131–139.
[15] D. Lebeugle, D. Colson, A. Forget, M. Viret, P. Bonville, J.F. Marucco, S. Fusil, Room temperature coexistence of large electric polarization and magnetic order in $BiFeO_3$ single crystals, Phys. Rev. B 76 (2007) 024116(1)–024116(8).
[16] D. Lebeugle, D. Colson, A. Forget, M. Viret, Very large spontaneous electric polarization in BiFeO3 single crystal at room temperature and its evolution under cycling fields, Appl. Phys. Lett. 91 (2007) 022907(1)–022907(3).
[17] W. Kaczmarek, Z. Pajak, M. Polomska, Differential thermal analysis of phase transitions in $(Bi_{1-x}La_x)FeO_3$ solid solutions, Solid State Commun. 17 (1975) 807–810.
[18] Y.E. Roginskaya, Y.Y. Tomashpolskii, Y.N. Venevtsev, V.M. Petrov, G.S. Zhdanov, The Nature of the dielectric and magnetic properties of BiFeO3, Sov. Phys. JETP 23 (1966) 47–51.
[19] V.V.S.S. Sai Sunder, A. Halliyal, A.M. Umarji, Investigation of tetragonal distortion in the $PbTiO_3$–$BiFeO_3$ system by high-temperature x-ray diffraction, J. Mater. Res. 10 (1995) 1301–1306.
[20] R. Gerson, P. Chou, W.J. James, Ferroelectric properties of $PbZrO_3$–$BiFeO_3$ solid solutions, J. Appl. Phys. 38 (1967) 55–58.
[21] R.T. Smith, G.D. Achenbach, R. Gerson, W.J. James, Dielectric properties of solid solutions of $BiFeO_3$ with Pb(Ti, Zr)O_3 at high temperature and high frequency, J. Appl. Phys. 39 (1968) 70–74.
[22] M.M. Kumar, A. Srinivas, S.V. Suryanarayana, T. Bhimasankaram, Dielectric and impedance studies on $BiFeO_3$–$BaTiO_3$ solid solutions, Phys. Status Solidi A 165 (1998) 317–326.
[23] J.P. Patel, A. Senyshyn, H. Fuess, D. Pandey, Evidence for weak ferromagnetism, isostructural phase transition, and linear magnetoelectric coupling in the multiferroic $Bi_{0.8}Pb_{0.2}Fe_{0.9}Nb_{0.1}O_3$ solid solution, Phys. Rev. B 88 (2013) 104108 (1)–104108(9).
[24] S. Matteppanavar, B. Angadi, S. Rayaprol, Single phase synthesis and room temperature neutron studies on multiferroic PbFe0.5Nb0.5O3, in: AIP Conference Proceedings, 1512, 2013, pp. 1232–1233.
[25] R.A. Brand, Improving the validity of hyperfine field distributions from magnetic alloys: part I: unpolarized source, Nuclear Instr. Meth. Phys. Res. B 28 (1987) 398–416.
[26] S. Matteppanavar, S. Rayaprol, K. Singh, V. Raghavendra Reddy, B. Angadi, Evidence for magneto electric and spin lattice coupling in $PbFe_{0.5}Nb_{0.5}O_3$ through structural and magnetoelectric studies, J. Mater. Sci. 50 (2015) 4980–4993.
[27] J. Patel, A. Singh, D. Pandey, Nature of ferroelectric to paraelectric phase transition in multiferroic $0.8BiFeO_3$–$0.2Pb(Fe_{1/2}Nb_{1/2})O_3$ ceramics, J. Appl. Phys. 107 (2010) 104115(1)–104115(7).
[28] D.P. Kozlenko, S.E. Kichanov, E.V. Lukin, N.T. Dang, L.S. Dubrovinsky, H. P. Lierman, W. Morgenroth, A.A. Kamynin, S.A. Grindev, B.N. Savenko, Pressure induced polar phases in relaxor multiferroic $Pb(Fe_{0.5}Nb_{0.5})O_3$, Phys. Rev. B 89 (2014) 174107(1)–174107(7).
[29] B. Mihailova, I.B. Maier, C. Paulmann, T. Malcherk, J. Ihringer, M. Gospodinov, R. Stosch, High temperature structural transformations in the relaxor ferroelectrics $PbSc_{0.5}Ta_{0.5}O_3$ and $Pb_{0.78}Ba_{0.22}Sc_{0.5}Ta_{0.5}O_3$, Phys. Rev. B 77 (2008) 174106(1)–174106(10).
[30] M.K. Singh, R.S. Katiyar, J.F. Scott, New magnetic phase transitions in $BiFeO_3$, J. Phys. Condens. Matter 20 (2008) 252203(1)–252203(4).
[31] R.K. Mishra, D.K. Pradhan, R.N.P. Choudary, A. Banerjee, Effect of yttrium on improvement of dielectric properties and magnetic switching behavior in $BiFeO_3$, J. Phys. Condens. Matter (2014) 045218(1)–045218(6).
[32] V. Singh, S. Sharma, M. Kumar, R.K. Kotnala, R.K. Dwivedi, Structural transition, magnetic and optical properties of Pr and Ti Co-doped $BiFeO_3$ ceramics, J. Magn. Magn. Mater. (2014) 264–267.